ISIJ International, Vol. 55 (2015), No. 2, pp. 392–398

Effect of Applied Voltage on the Current Density of CO_2 Electrolysis in High Temperature

Yoshiaki KASHIWAYA,[1)]* Yohei SHIOMI,[2)] Takahiro NOMURA[3)] and Masakatsu HASEGAWA[1)]

1) Dept. of Energy Science and Technology, Kyoto University, Yoshida Honmachi, Sakyo-ku, Kyoto, Kyoto-fu, 606-8501 Japan. 2) Graduate Student, Graduate School of Energy Science, Kyoto University, Yoshida Honmachi, Sakyo-ku, Kyoto, Kyoto-fu, 606-8501 Japan. 3) Hokkaido University, Center for Advanced Research of Energy and Materials, Hokkaido University, kita-13, Nishi-8, Kita-ku, Sapporo, Hokkaido, 060-8072 Japan.

(*Received on July 29, 2014; accepted on September 17, 2014*)

Reductions in CO_2 emission can be achieved directly through CO_2 capture and storage (CCS), a method that is particularly effective when used with large CO_2 emitters such as electrical power plants and iron and steel mills. Solid-oxide electrolysis presents an alternative means of reducing CO_2 that can use some of the CO_2 captured by CCS as a source of electrolysis. In addition, unused heat generated by steelmaking and through renewable sources (*e.g.*, solar and wind) can be utilized for high-temperature electrolysis.

This study investigated the effect of applying a high voltage of between 2.5 and 4.0 V to common electrolytic materials (YSZ and Pt), and found that although the initial current density of a new cell is very low, it increases drastically upon application of a high voltage. The results of FE-SEM observation revealed that the interface between the YSZ and Pt electrode moves into the YSZ by about 70 μm, and consists of a nano- and micro-porous structure that reduces the resistivity and gas diffusivity.

KEY WORDS: CO_2 electrolysis; YSZ; Pt electrode; high-performance cell.

1. Introduction

The reduction of CO_2 emissions is becoming an increasingly important issue in developing countries, as it offers a means of saving energy and generally increases the efficiency of machinery and industrial processes. On the other hand, CO_2 capture and storage (CCS) offers a direct method of reducing CO_2. This is of particular interest in Japan, where the direct discharge of CO_2 for both electrical power plants and steel mills amounts to ~44% of the total CO_2 emission in 2010. At present, CCS technology has all but reached practical application,[1)] essentially leaving only economic factors to be considered.

Solid-oxide electrolysis presents an alternative means of reducing CO_2, but can be used in conjunction with CCS by utilizing part of the CO_2 captured by CCS as a source of electrolysis. In addition, the unused heat generated in iron and steelmaking process (*e.g.* converter exhaust gases, molten slag[2)] and high temperature coke) allows for high-temperature electrolysis. Moreover, electricity generated through renewable energies such as solar and wind can be used as a buffer in terms of providing rapid increases in power generation on sunny and/or windy days, because the high-temperature electrolysis of CO_2 can produce CO and O_2 gases that can be used for energy storage.

High-temperature electrolysis has been mostly studied in the past in relation to the production of H_2 from H_2O, and thus most efforts have been directed toward the development of oxide materials with a high ionic conductivity. The most common oxide electrolyte has been $LaGaO_3$ (perovskite),[3)] and LaSrGaMgO (LSGM)[4)] oxide materials have also been well developed. The use of Ni as a cathode catalyst has also shown promise, leading to a number of Ni alloys being developed and studied.[5–8)] Although CO_2 electrolysis can be performed using similar techniques to H_2O electrolysis, it is complicated by the carbon deposition reaction that occurs in low the temperature region of between 600 and 700°C:

$$2CO_{(g)} = C_{(s)} + CO_{2(g)} \quad \text{..... (1)}$$

Consequently, there have been very few studies into CO_2 electrolysis;[9–15)] however, there has been much greater interest in the co-electrolysis of CO_2 and H_2O[16–19)] due to the greater thermodynamic simplicity of H_2O electrolysis and the fact that the inverse water gas shift reaction can convert CO_2 to H_2O.

In this study, a conventional yttria-stabilized-zirconia (YSZ) solid electrolyte was used to assess the viability of utilizing the high temperature (1 000 to 1 500°C) exhaust gas generated by iron and steel making. Platinum was selected for both the cathode and anode, as although it is expensive, it can also be recycled completely. Since an increase in the performance of electrolysis has been previously identified when applying an overpotential from 2.5 to 4.0 V, this was investigated further with a view to identifying the cause.

* Corresponding author: E-mail: kashiwaya@energy.kyoto-u.ac.jp
DOI: http://dx.doi.org/10.2355/isijinternational.55.392

2. Experimental

2.1. Reaction System and Thermodynamic Consideration

Figure 1 shows a thermodynamic evaluation of the CO_2–CO system, from which the equilibrium potential (E(V)) can be calculated using the Nernst equation ($E = -\Delta G°/nF$, where $\Delta G°$ represents the standard Gibbs free energy of reaction). Although three reactions are considered (Eqs. (2)–(4)), Eq. (4) rarely occurs as a single step due to the adsorption of CO_2(g) at the oxygen atom.

$$CO_{2(g)} \rightarrow CO_{(g)} + 1/2\, O_{2(g)} \quad \text{..... (2)}$$

$$CO_{(g)} \rightarrow C_{(s)} + 1/2\, O_{2(g)} \quad \text{..... (3)}$$

$$CO_{2(g)} \rightarrow C_{(s)} + 1/2\, O_{2(g)} \quad \text{..... (4)}$$

Based on Reactions (2) and (3), equilibrium potentials were evaluated and are compared in Fig. 1. Below 700°C, Reaction (3) will be dominant, resulting in carbon deposition on the surface of the electrode and a retardation of the overall reaction rate. In the high-temperature region above 700°C, Reaction (2) becomes dominant and is the most relevant to the present study. This differs from H_2O electrolysis, in which it is favorable to conduct electrolysis at as low a temperature as possible. For instance, Ishihara *et al.*[3] based their results on a temperature of 600°C. However, such temperatures make CO_2 electrolysis quite difficult to perform, and so the lowest temperature of 800°C was selected in this study. Furthermore, given that the resistances of the cell and YSZ itself also significantly decrease at higher temperature, the performance of electrolysis should drastically increase.

Figure 2 shows the reaction system used, in which the main reaction is represented by Eq. (2), the cathode reaction is expressed by Eq. (5) and the anode reaction is Eq. (6).

$$\text{Cathode: } CO_2 + 2\,e^- \rightarrow CO + O^{2-} \quad \text{..... (5)}$$

$$\text{Anode: } O^{2-} \rightarrow 1/2\, O_2(g) + 2\,e^- \quad \text{..... (6)}$$

2.2. Apparatus and Procedure

The electrolytic cell used was a Tammann-type YSZ tube (8 mol%Y_2O_3, 8 × 5 mmf × 50 mmL, Nikkato, Co. Ltd.), a cross section and side view of which is provided in **Fig. 3**. The Pt electrodes were 20–30 μm in thickness, and in the case of cathode, had an area of 1 cm^2. The actual area of the anode was difficult to fix, and so only the position directly opposite the cathode was confirmed. Although a geometrical area of anode is less than that of the cathode and 0.625 cm^2 (inner diameter: 0.5 cm), the slightly larger area was put on the side of anode. After drying the Pt (TR-7061, Tanaka Kikinzoku Kogyo, Co. Ltd.) pasted on the electrodes position, the cell was heated to 1 000°C and held 2 hours to evaporate the organic compound and fix the thin Pt plate to the YSZ surface. The structure of the Pt electrode was observed by laser microscopy and FE-SEM before and after experimentation. These results, and their relationship to electrolysis, will be published in the following paper.

The anode gas was introduced by an alumina tube (4×2 mmϕ ×100 mmL), around which a Pt wire (0.5 mmϕ) was wound for three to four turns to ensure good contact. Since the inner diameter of cell is 5 mm, and outer diameter of the alumina tube is 4 mm, the 0.5 mm diameter Pt wire and the anode electrode from 20 to 30 μm in thickness can be made a good contact.

Figure 4 shows a schematic diagram of the reaction furnace and quartz tube setting the electrolytic cell. Three different aluminum gas-sealing caps were used to connect the quartz reaction tube, YSZ cell and the alumina tube of the anode gas inlet, all of which were sealed by O-rings. The small electric furnace measured 30 mm in width and was heated using a Pt element wire to produce a uniform

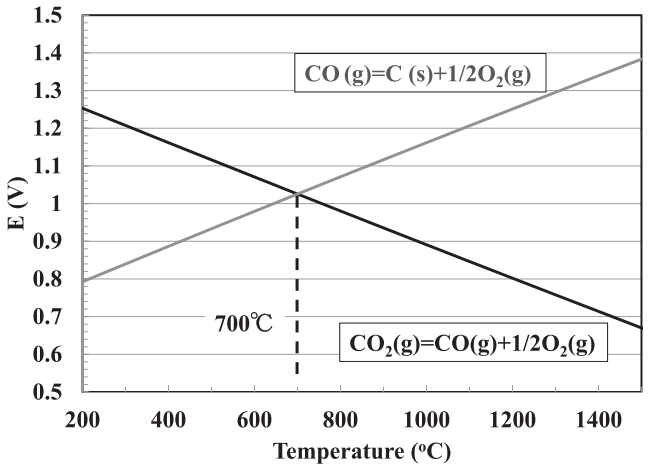

Fig. 1. Thermodynamic evaluation on the reactions of CO_2 and CO decomposition.

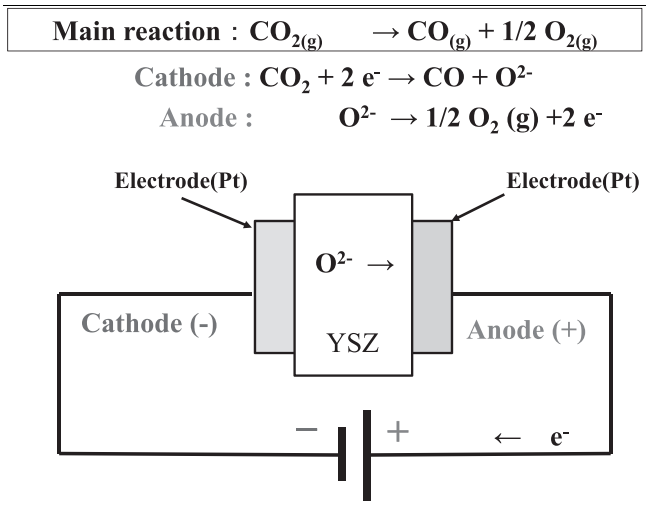

Fig. 2. Reaction system in the present study.

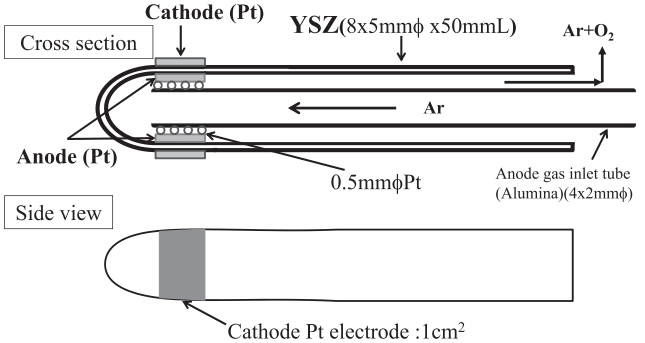

Fig. 3. Cross section and side view of Tammann type YSZ.

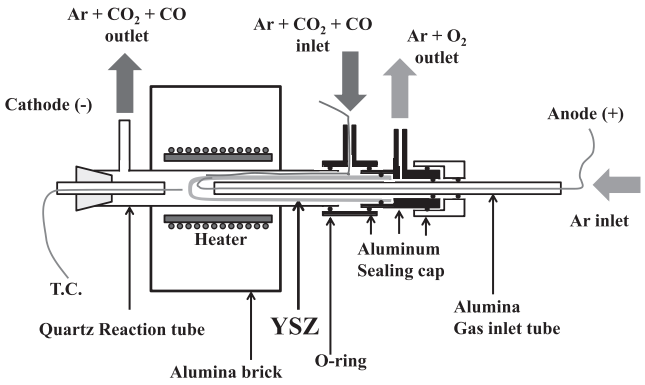

Fig. 4. Schematics of reaction furnace and quartz tube setting the electrolytic cell.

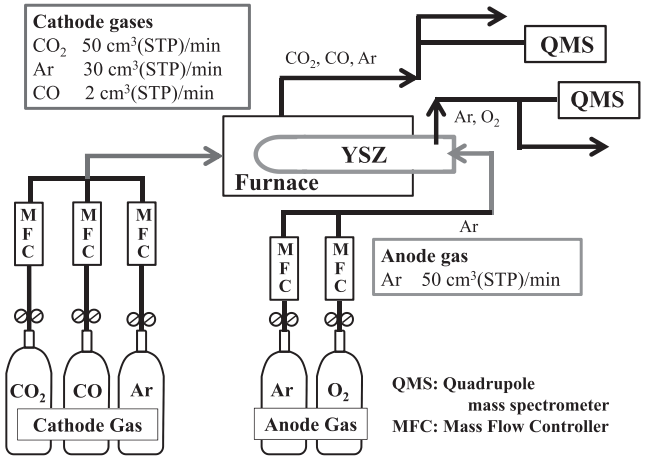

Fig. 5. Schematics of experimental apparatus.

temperature zone (±5°C) of about 10 mm. This width was considered sufficient given that the 4 mm width of the Pt electrodes means a cathode area of 1 cm^2.

Figure 5 shows a schematic of the experimental apparatus used, in which cathode gases (Ar, CO_2, CO) and anode gas (Ar) were controlled separately by means of a MFC (mass flow controller) and the outlet gases were analyzed by QMS (quadrupole mass spectrometry). In the case of the anode gas analysis, the calibrating the QMS was performed by adding O_2 gas to Ar, while QMS calibration for the cathode gas was performed by suitably changing the gas composition using the three MFCs. A detailed description of this calibration method has been previously reported.[20)]

2.3. Experimental Conditions

The gas composition used in the cathode was Ar:50 cm^3 (STP)/min, CO_2:30 cm^3 (STP)/min, CO:2 cm^3 (STP)/min, which equates to 36% CO_2 and 2% CO. The anode gas was an ultra-high purity Ar (> 99.9999%) at 50 cm^3 (STP)/min. The linear velocity of the cathode gas near the electrode was about 1.67 cm/s, and was 11 cm/s at the anode.

Table 1 provides a summary of the experimental conditions used for the four separate experiments (EXP-1, EXP-2, EXP-3 and EXP-4) that were performed to clarify the effect of an applied voltage on the performance of an electrolytic cell. Since the experimental conditions are somewhat complicated, the concept was explained using **Fig. 6**, in which the basic sequence of voltage variation is illustrated. From a preliminary experiment, it was found that the performance of the cell does not change until at least 2.0 V, on the basis of which the voltage range was divided into two regions: 1.4 to 2.0 V (Voltage-1) and 2.5 to 3.5–4.0 V (Voltage-2). In Table 1, the term 'No.' refers to the order of the experiment and 'Notation' defines the temperature its relative order. The last term, 'Current', refers to the current when 2 V is applied.

The basic experimental set, as shown in Fig. 6, consisted of Voltage-1, Voltage-2 and Voltage-1. Using this experimental set, the effect of high voltage (voltage-2) can be measured.

The experimental temperature was varied between three levels: 800, 900 and 1 000°C. All Voltage-2 experiments, with the exception of EXP-4, were carried out at 1 000°C (Table 1(c)).

In EXP-1, following T1000-1 and T1000-2, experiments were conducted at 900°C (T900-1) and 800°C (T800-1). The Voltage-2 was applied at T1000-0, then, the effect of overpotential on the cell performance was examined at T1000-1, T900-1 and T800-1. In EXP-2, three test were performed at Voltage-2 (T1000-2, T1000-3 and T1000-4), and the effect of each set of conditions on the cell performance was measured at T1000-5. In EXP-3, after one set of T1000-6 and T1000-7, the stability of cell performance was measured several times at 1 000, 900 and 800°C (T900-2→T800-2→T900-3→T1000-8). Finally in EXP-4, the effect of applying Voltage-2 (T1000-9 and T1000-10) was measured by T1000-11; and in T800-3, Voltage-2 was applied at 800°C to provide a comparison with 1 000°C, and the effect was measured in T800-4.

3. Results and Discussion

3.1. Effect of High Voltage (2.5–4.0 V) on Current Density

Figure 7 shows the typical experimental results obtained at 1 000, 900 and 800°C, in which a voltage of between 1.4 and 2.0 V was applied at a 0.2 V step interval at Voltage-1. This shows a corresponding increase in the current density and the evolution of CO gas. Using the known current, the gas flow rate for CO can be evaluated from Faraday's equation(Eq. (7)) based on Eq. (5):

$$\Delta V_{\text{CO by Faraday}}\left(\text{cm}^3\left(\text{STP}\right)/\text{min}\right) = \text{I}\left(\text{A}\right)\times 60\times 22\,414/\left(\text{nF}\right) \quad \text{..... (7)}$$

where n is the number of electrons (= 2) and F is the Faraday constant (= 96 485 C/mol).

Through gas analysis, the differences in CO_2 (ΔV_{CO_2}) and CO (ΔV_{CO}) gas flow rates can be evaluated:

$$\Delta V_{CO_2}\left(\text{cm}^3\left(\text{STP}\right)/\text{min}\right) = \left[CO_2\right]\text{out} - \left[CO_2\right]\text{in} \quad \text{... (8)}$$

$$\Delta V_{CO}\left(\text{cm}^3\left(\text{STP}\right)/\text{min}\right) = \left[CO\right]\text{out} - \left[CO\right]\text{in} \quad \text{..... (9)}$$

The CO_2 electrolysis causes CO_2 to decrease and CO to increase, leading to a negative ΔV_{CO_2} and positive ΔV_{CO} in Fig. 7. It was found that the measured ΔV_{CO} and that obtained by the Faraday equation are almost the same, which means that the current efficiency was almost 100%.

From 2.5 V to 4.0 V, the proportion of electron conduc-

Table 1. (a) Experimental conditions for EXP-1 and EXP-2. (b) Experimental conditions for EXP-3. (c) Experimental conditions for EXP-4.

(a)

	EXP-1				EXP-2	
No.	1	2	3	4	5, 6, 7	8
Notation	T1000-0	T1000-1	T900-1	T800-1	T1000-2,3,4	T1000-5
Temp. (°C)	1 000°C	1 000°C	900°C	800°C	1 000°C	1 000°C
Voltage-1 (step)	1.4–2.0 V (0.2 V, 5 min)	1.4–2.0 V (0.2 V, 5 min)	1.4–2.0 V (0.2 V, 5 min)	1.4–2.0 V (0.2 V, 5 min)	1.4–2.0 V (0.2 V, 5 min)	1.4–2.0 V (0.2 V, 5 min)
Voltage-2 (step)	2.5–4.0 V (0.5 V, 5 min)	—	—	—	2.5–3.5 V (0.5 V, 5 min)	—
Current (at 2 V)	33 mA	61 mA	25 mA	15 mA	78, 161, 287 mA	318 mA

(b)

	EXP-3					
No.	9	10	11	12	13	14
Notation	T1000-6	T1000-7	T900-2	T800-2	T900-3	T1000-8
Temp. (°C)	1 000°C	1 000°C	900°C	800°C	900°C	1 000°C
Voltage-1 (step)	1.4–2.0 V (0.2 V, 5 min)	1.4–2.0 V (0.2 V, 5 min)	1.4–2.0 V (0.2 V, 5 min)	1.4–2.0 V (0.2 V, 5 min)	1.4–2.0 V (0.2 V, 5 min)	1.4–2.0 V (0.2 V, 5 min)
Voltage-2 (step)	2.5–3.5 V (0.5 V, 5 min)	—	—	—		—
Current (at 2 V)	309 mA	356 mA	189 mA	96 mA	193 mA	340 mA

(c)

	EXP-4			
No.	15, 16	17	18	19
Notation	T1000-9, 10	T1000-11	T800-3	T800-4
Temp. (°C)	1 000°C	1 000°C	800°C	800°C
Voltage-1 (step)	1.4–2.0 V (0.2 V, 5 min)	1.4–2.0 V (0.2 V, 5 min)	1.4–2.0 V (0.2 V, 5 min)	1.4–2.0 V (0.2 V, 5 min)
Voltage-2 (step)	2.5–3.5 V (0.5 V, 5 min)	—	2.5–4.0 V (0.5 V, 5 min)	—
Current (at 2 V)	338, 381 mA	390 mA		

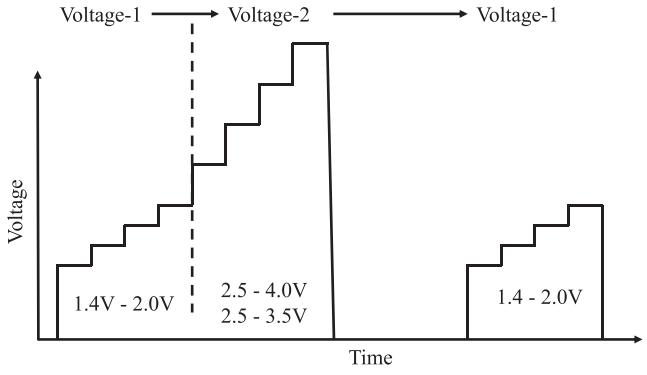

Fig. 6. Illustration of basic experimental conditions for clarifying the effect of Voltage-2.

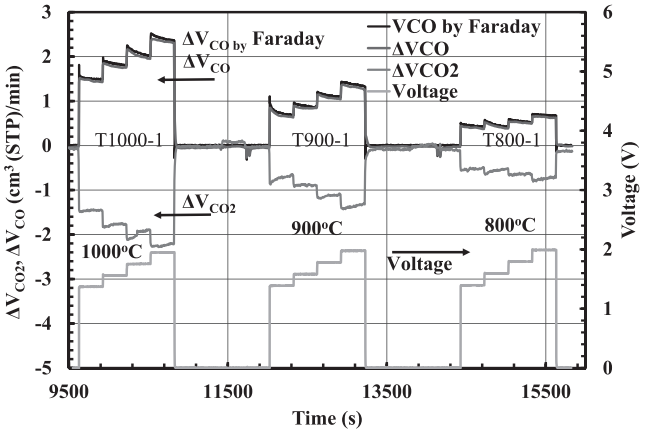

Fig. 7. Typical experimental results of 1 000°C, 900°C and 800°C.

tivity increased, and at the maximum voltage 3.5 or 4.0 V, the current increased drastically, but the gas evolution decreased oppositely. The phenomenon leads to a cell breakage, when the experiment continued a long time. However, since the maximum voltage application at 3.5 or 4.0 V was within 10 min in this experiment, the cell could be used safely in the lower voltage region (Voltage-1). In addition, a reduction of ZrO_2 might occur from more than 2 V thermodynamically. However, the reoxidation of the reduced Zr

by CO_2 will occur simultaneously ($Zr + 2CO_2(g) = ZrO_2 + 2CO(g)$). The reoxidation will sometime connect to a decomposition of solid solution of YSZ (ZrO_2-8mol%Y_2O_3). When the decomposition become significant, the color of YSZ turn to black, but the color returned again to white under the usage of lower voltage experiment.

The transient response phenomenon was observed on the variation of current density and the evolution of gas, when a voltage increased. This phenomenon can be understand by the measurement of AC impedance spectroscopy and the analysis through a CR(capacitor and resistor) equivalent circuit. When the reaction mechanism can be expressed by the combination of some CR parallel circuits, the current profile at DC voltage application will vary from highest value to a lower stable value. The phenomena is corresponding to a charging of C(capacitor). In this study, the current measurement was carried out at the stable point of the current variation at each constant voltage.

The relationship between voltage (V) and current density (A/cm^2) was measured, and the associated increase in current density is shown in **Fig. 8**. In EXP-1, T1000-0 was the first measurement obtained with a new cell, and therefore always exhibited a significantly lower current density. Thus, all results other than T1000-0 are shown for Voltage-2 in Fig. 8. In the case of EXP-2, the Voltage-2 was applied at T1000-2, T1000-3 and T1000-4, then, the effect of Voltage-2 was measured by T1000-3, T1000-4 and T1000-5. Although T1000-1 showed the lowest amount of increase, T1000-3 showed the greatest increase as a result of the Voltage-2 conditions in T1000-2 (this information is not shown in Fig. 8). The irregular point at 2 V in T1000-3 might be an experimental error, so that the measurement was started before OCV (open circuit voltage) did not become a stable. The time for getting a stable OCV (from 400 mV to 500 mV in this experiment) was about 10 min, however, sometime, it took about 20–30 min. The error might come from the difference of waiting time. T1000-4 also shows a significant increase over T1000-3. From T1000-5 to T1000-10, there was only a relatively minor increase in current density. Finally, the difference between T1000-10 and T1000-11 in EXP-4 was almost zero, which meant that the cell reached a steady state at a maximum voltage of 3.5 V. The increase in the current density from T1000-0 to T1000-11 was about 30 times at 1.4 V and 12 times at 2 V. The significant increase in the current density was obtained by the application of Voltage-2. The internal resistances estimated from the slope of I-V curves were quickly decreased from 23 Ω at T1000-0 to 5.6 Ω at T1000-3 and gradually decreased to 3.5 Ω at T1000-11.

From these results, it is considered that physical condition of cell will be changed by a high voltage (Voltage-2), which result in an increase in current density. The change is related to a broken of the interface between Pt electrode and YSZ surface, and a rearrangement of the interface. The detail of the rearrangement of the interface was examined by FE-SEM and explained in the later section. The amount of change will decrease with time and close to a steady state according to a maximum voltage.

Figure 9 shows the IR drop at each applied voltage in the experiment of 1 000°C. According to the increase in the current density, the IR drop also increased. The maximum IR drop at T1000-11 was 0.04 V at the application of 1.4 V and 0.07 V at the one of 2 V. Unfortunately, a reference electrode could not be used in the present experiment, the IR drops in the cathode and the anode could not classified. The internal resistance consists of a resistance of YSZ (R_{YSZ}) and charge transfer (Rct) which can be measured by AC impedance method. The resistance of contact can be neglected except the new cell (T1000-0) in the present experiment. According to the increase in cell performance from T1000-1 to T1000-11, the proportion of Rct decreases significantly, while the value of R_{YSZ} slightly decreased after the applying the Voltage-2, which meant a surface of YSZ was broken and the thickness of YSZ became thin. So that the proportion of R_{YSZ} became larger at T1000-11 (the details will be reported elsewhere), the large IR drop in T1000-11 will be resulted from the resistance of YSZ (R_{YSZ}), which is corresponding to a resistance of ionic transfer (O^{2-}) in the electrolyte.

Figure 10 shows the relationship between voltage and current density for EXP-1, in which the performance of cell was very low and the data quite scattered when compared with the results of EXP-3 and EXP-4. In addition, the accuracy of current measurement less than 10 mA is relatively low in this experiment, so that the data in lower voltage rage (1.4 V and 1.6 V) was intersect between 800 and 900°C, which was within a range of error.

The variation in current density with temperature was also non-linear, but became linear as the number of experiments increased. On the other hand, in EXP-2 (Fig. 8, Table

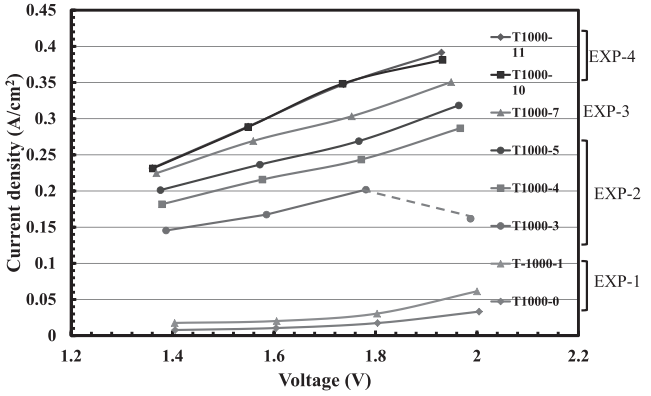

Fig. 8. Relationship between voltage and current density in 1 000°C.

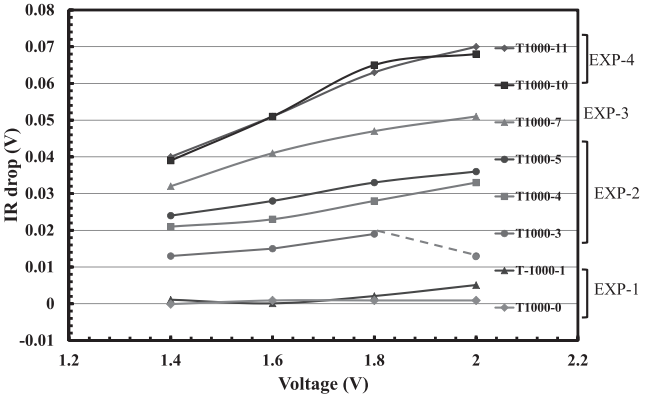

Fig. 9. Relationship between voltage and current density for EXP-1.

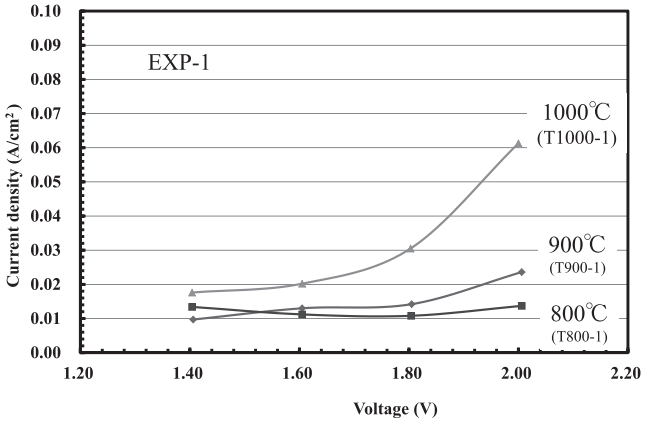

Fig. 10. Variation of IR drop at each applied voltages in 1 000°C.

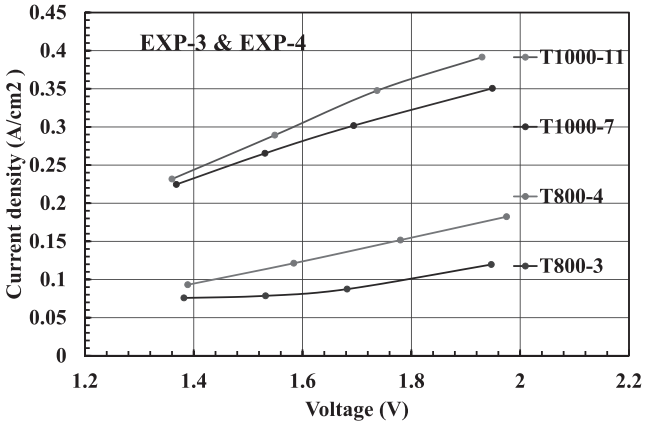

Fig. 12. Relationship between voltage and current density for EXP-3 and EXP-4.

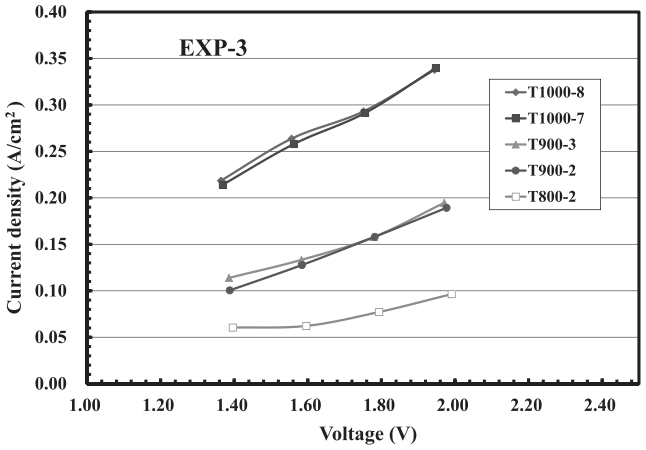

Fig. 11. Relationship between voltage and current density for EXP-3.

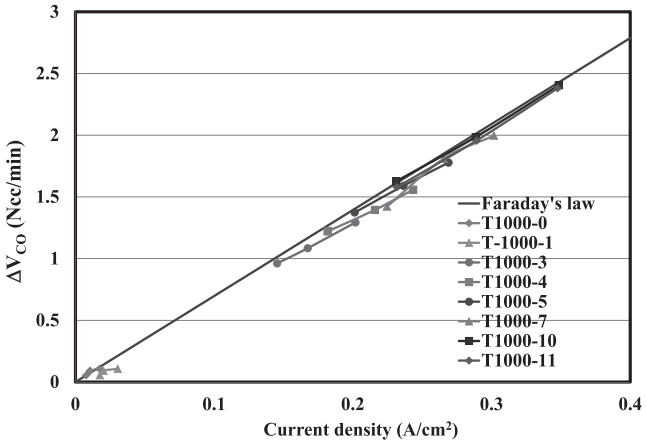

Fig. 13. Comparison of current densities with Faraday's law.

1(a)), the results were expected to increase drastically by applying Voltage-2 in T1000-2, T1000-3 and T1000-4. In the EXP-1 and EXP-2, the cell condition was in the course of activating, then, the scattering of data was relatively large and the point of T1000-3 at 2 V was largely deviated from the consistency as mentioned above (Fig. 8).

Figure 11 shows the results of EXP-3, in which no Voltage-2 was applied. The order of this experiment was T1000-7→T900-2→T800-2→T900-3→T1000-8, with the high reproducibility of the results indicating that a voltage of less than 2 V clearly has little effect on the cell conditions. To confirm this assumption, Voltage-2 was again applied to T1000-9 and T1000-10 in EXP-4, and the variation in current density was measured in T1000-11 (**Fig. 12**). The current densities obtained at 2 V from T1000-7 to T1000-9 were 356, 340 and 338 mA, respectively, which were either almost constant or slightly decreased (Table 1 (EXP-3 & EXP-4)). However, the current density again increased from T1000-9 to T1000-10 because of the Voltage-2 in T1000-9. This found no difference between T1000-10 and T1000-11 (Fig. 8), which means that the Voltage-2 in T1000-10 had no further effect on the cell conditions.

In Fig. 12, only the results for T1000-7 and T1000-11 are shown because T1000-8 and T1000-9 were almost the same as T1000-7, and T1000-10 was the same as T1000-11.

The effect of Voltage-2 was further examined at 800°C in experiments T800-3 and T800-4. As shown in Fig. 12, when Voltage-2 was applied in T800-3, the current density in T800-4 increased. This suggests that the effect of high-voltage may change be influenced by temperature, and it is considered that there must be some threshold value to the temperature and voltage related conditions. That is, when these conditions exceed the threshold, the current density again increases. However, further systematic investigation is still needed to clarify this in more detail.

Figure 13 shows the relationship between ΔV_{CO} (Eq. (9)) and current density at 1 000°C in comparison with Faraday's law($\Delta V_{CO\ by\ Faraday}$ (Eq. (7)). This demonstrates that the current efficiency was almost 100%, which means that the electrical input was almost entirely consumed by gas evolution.

Figure 14 shows the interface between the YSZ and Pt electrode, as observed by FE-SEM before and after experimentation. The before sample was heat treated at 1 000°C under air, as mentioned in Section 2.2, but was not subjected to electrolysis. As can be seen, this results in a straight interface that is effectively unaltered. In contrast, the after sample was subjected to electrolysis up to a maximum of 4.0 V, which was found to produce a significant increase in cell performance. Afterelectrolysis, the sample was embedded in resin, sectioned to expose the interface, and then polished with 1 μm diamond paste and finished to a mirror surface by colloidal alumina. As shown in Fig. 14, electrolysis clearly causes the interface to move toward the inside of the YSZ to a maximum depth of 70 μm. The front of this inter-

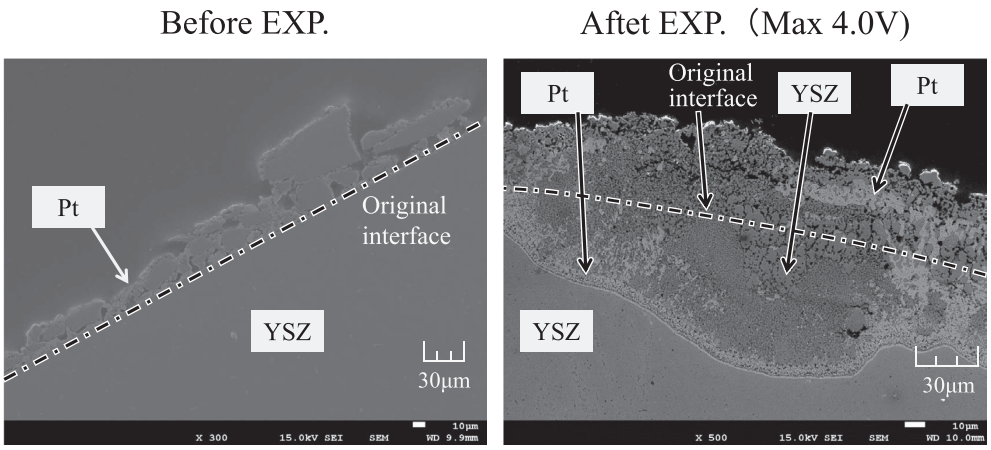

Fig. 14. Cross sectional image of interface between YSZ and Pt electrode before and after experiment.

face, evident as a line less than 1 μm in width, has a nano-porous structure that will be described in more detail in the following paper. Behind this nano-porous line, a micro-porous and mixed structure of Pt and YSZ is present. This overall structure is believed to be capable of reducing the resistivity and gas diffusivity, thereby increasing the cell performance and current density. The structural change itself is attributed to a destruction of the YSZ surface by high voltages, and the subsequent migration of Pt toward the front of the interface.

4. Conclusions

By combining YSZ with a Pt electrode, both of which are considered ordinary materials, an increase in current density was achieved during CO_2 electrolysis when a high voltage of 2.5 to 4.0 V was applied. The results obtained from this can be summarized as follows:

(1) The low performance of a new cell in terms of current density can be drastically improved by applying a voltage of 2.5 to 4.0 V. Finally, the current density was about 30 times at 1.4 V and 12 time at 2.0 V.

(2) Cell performance reaches a steady state when conditions of temperature and voltage are constant condition, but increases if either of these conditions exceeds a threshold value.

(3) The interface between YSZ and Pt electrode moves toward the inside of YSZ during electrolysis by about 70 μm when a maximum of 4.0 V is applied. The front of this interface consists of a thin line of nano-porous Pt, behind which is mixed microstructure of porous Pt and YSZ that is believed to reduce the resistivity and gas diffusivity at the interface.

Acknowledgement

A part of this research was supported by Grant-in-Aid for Scientific Research B, (No. 24561010), Japan Society for the Promotion of Science (JSPS).

REFERENCES

1) Home page of Japan CCS, Co., Ltd.: http://www.japanccs.com, (accessed 2014-07-18).
2) Y. Kashiwaya, Y. In-Nami and T. Akiyama: *ISIJ Int.*, **50** (2010), 1245.
3) T. Ishihara and T. Kanno: *ISIJ Int.*, **50** (2010), 1291.
4) T. Ishihara, H. Matsuda and Y. Takita: *J. Am. Chem. Soc.*, **116** (1994), 3801.
5) R. Accorsi and E. Bergmann: *J. Electrochem. Soc.*, **127** (1980), 804.
6) A. Brisse, J. Schefold and M. Zahid: *Int. J. Hydrogen Energ.*, **33** (2008), 5375.
7) T. Ishihara, J. W. Yan, M. Shinagawa and H. Matsumoto: *Electrochim. Acta* **52** (2006), 1645.
8) S. H. Jensen, P. H. Larsen and M. Mogensen: *Int. J. Hydrogen Energ.*, **32** (2007), 3253.
9) S. D. Ebbesen and M. Mogensen: *J. Power Sources*, **193** (2009), 349.
10) R. D. Green, C-C. Liu and S. B. Adler: *Solid State Ionics*, **179** (2008), 647.
11) J. Mizusaki and H. Tagawa: *Solid State Ionics*, **53–56** (1992), 126.
12) F. Bidrawn, G. Kim, G. Corre, J. T. S. Irvine, J. M. Vohs and R. J. Gorte: *Electrochem. Solid St.*, **11** (2008), B167.
13) G. Tao, K. R. Sridhar and C. L. Chan: *Solid State Ionics*, **175** (2004), 615.
14) G. Tao, K. R. Sridhar and C. L. Chan: *Solid State Ionics*, **175** (2004), 621.
15) K. R. Sridhar and B. T. Vaniman: *Solid State Ionics*, **93** (1997), 321.
16) Z. Zhan and L. Zhao: *J. Power Sources*, **195** (2010), 7250.
17) W. Li, Y. Shi, Y. Luo and N. Cai: *J. Power Sources*, **243** (2013), 118.
18) S. H. Jensen, X. Sun, S. D. Ebbensen, R. Knobble and M. Mogensen: *Int. J. Hydrogen Energ.*, **35** (2010), 9544.
19) S. D. Ebbensen and M. Mogensen: *J. Power Sources*, **193** (2009), 349.
20) Y. Kashiwaya and M. Watanabe: *ISIJ Int.*, **52** (2012), 1394.